

## Effect of multiphoton processes on the asymmetric fluorescence spectrum and spectral correlations of a two-level atom driven bichromatically by two strong laser fields

Su-jing Liu,<sup>1,2</sup> Xu-xing Geng<sup>1</sup>, Ming Xue<sup>1</sup>, and Gao-xiang Li<sup>1,\*</sup>

<sup>1</sup>Department of Physics, Huazhong Normal University, Wuhan 430079, China

<sup>2</sup>School of Physics and Optoelectronic Engineering, Yangtze University, Jingzhou 434023, China



(Received 26 May 2023; accepted 21 September 2023; published 6 October 2023)

We focus on the influence of multiphoton effect on the fluorescence spectrum and photon statistics of the bichromatically driven two-level atomic system. The influence of the multiphoton effect of the weaker driving field on the system and spontaneous emission are revealed by Schrieffer-Wolff perturbation theory, respectively. The physical origin of the multiphoton process affecting the fluorescence spectral asymmetry characteristics is fully investigated by studying the population distribution and the dressed atomic transition weight. Further, the suppression condition of the central peak of the central band is investigated. The photon statistical properties of the system are revealed by studying the frequency-resolved correlations between different sidepeaks and the central peak and sidepeak, respectively. In particular, the physical picture of the asymmetry of the two-photon correlation signal that is affected by the multiphoton process of the weaker driving field affecting the timing detection is fully revealed by the two methods of correlation moment and conditional quantum state, respectively. These results of ours provide a theoretical approach for studying multiphoton processes in multichromatically driven quantum systems, as well as for developing quantum simulation techniques such as spin locking.

DOI: [10.1103/PhysRevA.108.043105](https://doi.org/10.1103/PhysRevA.108.043105)

### I. INTRODUCTION

It is well known that study of the fluorescence spectrum is not only an excellent platform for understanding atom-light interactions but also provides a feasible method for the preparation of single photon sources [1,2], quantum sensing [3] in quantum information [4]. In the last two decades, due to the experimental research of artificial atoms, such as quantum dots [5–11], superconducting qubits [12], and nitrogen-vacancy centers [13], the study of the fluorescence spectrum has attracted renewed interest. In particular, the fluorescence spectrum of bichromatically driven two-level atomic systems has been well studied both experimentally [9,14,15] and theoretically [16–18], mainly due to the existence of richer spectral features than monochromatically driven systems.

The two-level atom driven by a bichromatic field exhibits a range of nonlinear and multiphoton dynamics of light-matter interaction [19,20]—that is what we focus on. The fluorescence spectrum has been calculated for equal-amplitude field components symmetrically or asymmetrically detuned from the atomic frequency, and components having unequal amplitudes [18,21–28]. In these studies, basically most researchers only considered the perturbation of the system by the weaker driving field when analytically calculating the fluorescence spectrum while ignoring its multiphoton correction for spontaneous emission, so that the spectrum has obvious symmetry. This is limited because the high-resolution spectroscopy recently obtained by Gustin *et al.* [29] by an InGaAs quantum

dot driven bichromatically by two strong coherent fields is inherently asymmetric. However, no clear analytical explanation has been given for the asymmetry of the spectrum. To solve this issue we apply the Schrieffer-Wolff perturbation theory (SWPT) [30,31] to deal with the effective Hamiltonian and spontaneous emission of two-level atomic systems driven by a strong bichromatic field and give analytical expression for the generation of the asymmetric spectrum. This analytical solution basically agrees with the numerical results of Ficek and Freedhoff [18], and also reveals the physical origin of the asymmetric spectrum of the experimental results of Gustin *et al.* [29]. Meanwhile, the multiphoton correction [32] of the system and spontaneous emission by the weaker driving field, and the resulting asymmetric high-order harmonic spectrum, provide a feasible route for high-order harmonic generation (HHG) [33–35]. One of the most important applications is the generation of attosecond pulses [36].

Can the multiphoton process accompanied by the system correction by the weaker driving field provide a feasible solution for the preparation of a multiphoton nonclassical state? To answer that question it is particularly important to analyze the statistical properties of photon among the high-order harmonic spectral components. Most previous studies on frequency-filtered photon correlation of fluorescence have focused on single-laser driving field [37–40]; few researchers focused on the bichromatic driving field [35,41]. The optical cavity weakly coupled with the system is used to simulate the Lorentz filter [42], and the physical origin of the asymmetric photon statistical signal is revealed.

In this paper we investigate the influence of the multiphoton process on the fluorescence spectrum and photon statistics by a bichromatically driven two-level atomic system.

\*gaox@ccnu.edu.cn

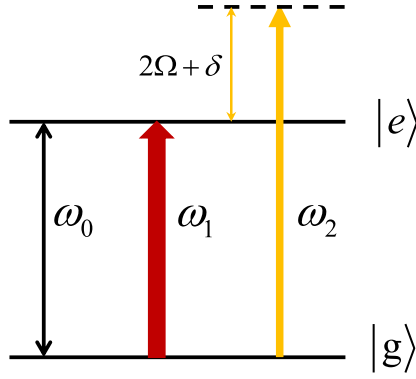


FIG. 1. System consisting of a two-level atom driven by a bichromatic field with different amplitudes and frequencies.

To reveal the physical nature of the weaker driving field affecting the spectral characteristics of the system, the effective Hamiltonian of the system, the spontaneous emission after multiphoton correction, the population distribution, and the fluorescence spectrum under different conditions are deduced, respectively. To investigate the frequency-resolved correlation characteristics of the system, the time-domain photon correlation signals between different components of the fluorescence spectra are studied. The paper is structured as follows: In Sec. II we describe the theoretical model that produces asymmetric high-order harmonic resonance fluorescence, and at the same time, the physical mechanisms of the asymmetry of the spectrum are discussed. In Sec. III, the frequency-resolved correlation features of different spectral combinations are discussed. The correlation moment method and conditional quantum state are used to analyze the asymmetry that occurs in the correlation signal. Finally, we conclude our discussion in Sec. IV.

## II. BICHROMATIC LASER-DRIVEN TWO-LEVEL SYSTEM AND FLUORESCENCE SPECTRUM

### A. Theoretical model

We consider the two-level atom with excited state  $|e\rangle$  and ground state  $|g\rangle$  separated with frequency  $\omega_0$ , which is driven by a bichromatic laser field (see Fig. 1) with different amplitudes and frequency components  $\omega_1$  and  $\omega_2$ . The Rabi frequencies of the coupling between the bichromatic field and the atom are  $2\Omega_1$  and  $2\Omega_2$  ( $\Omega_1 > \Omega_2$ ), respectively. The Rabi frequency ratio of the two components of the bichromatic field is  $\alpha = \Omega_2/\Omega_1$ . The strong driving field resonates with the atomic transition frequency, i.e.,  $\omega_1 = \omega_0$ . In the rotating frame with the frequency  $\omega_1$  of the strong laser field, the Hamiltonian of the system is given by

$$H_{AL} = \Omega_1(\sigma_+ + \sigma_-) + \Omega_2(\sigma_+ e^{-i\Delta t} + \sigma_- e^{i\Delta t}), \quad (1)$$

in which  $H_{AL}$  describes the interaction of the atom with the bichromatic driving field. The transition operator is  $\sigma_- = \sigma_+^\dagger = |g\rangle\langle e|$ . The detuning of the weaker field and the atomic transition frequency are  $\Delta = \omega_2 - \omega_1$  with the relationship  $\delta = \omega_2 - \omega_1 - 2\Omega(|\delta| \ll 2\Omega)$ .

To gain further insight, the system enters the first dressed representation of the strong field interacting with the atom.

The eigenvalues and eigenstates of this representation are  $\pm\Omega$  and  $|\pm\rangle = \frac{1}{\sqrt{2}}(|g\rangle \pm |e\rangle)$ , respectively. The first dressed transformation  $U_{d1}$  is introduced [43]

$$U_{d1} = \frac{1}{\sqrt{2}} \begin{bmatrix} 1 & -1 \\ 1 & 1 \end{bmatrix}, \quad (2)$$

and the Hamiltonian in the first dressed representation is obtained by  $H'_{AL} = U_{d1}^\dagger H_{AL} U_{d1}$ , i.e.,

$$H'_{AL} = \Omega R_z + \frac{\Omega_2}{2} [(R_z + R_+ - R_-) e^{-i\Delta t} + \text{H.c.}], \quad (3)$$

in which  $R_z = |+\rangle\langle +| - |-\rangle\langle -|$  is the atomic inversion operator and  $R_- = R_+^\dagger = |-\rangle\langle +|$  are the transition operators in the first dressed representation. After unitary transformation  $U_\Omega = e^{-2iR_z t}$ , the Hamiltonian in the interaction picture of the first dressed representation is obtained by

$$H'_1 = \frac{\Omega_2}{2} [R_z (e^{-2i\Omega t} + e^{2i\Omega t}) - R_- e^{-4i\Omega t} - R_+ e^{4i\Omega t}] + \frac{\Omega_2}{2} (R_+ + R_-) + \frac{\delta}{2} R_z. \quad (4)$$

To reveal the multiphoton effect of the weaker driving field on the system and spontaneous emission, the Hamiltonian Eq. (4) will be dealt with in the following perturbation theory.

### B. Multiphoton correction of system with weaker driving field

In general, when the intensity of the weaker component of the driving field is much smaller than the strong one ( $\alpha \ll 1$ ), the time-dependent term of the Hamiltonian in Eq. (4) can be ignored by applying the rotating-wave approximation. However, when  $\Omega_2$  is strong and  $\alpha \ll 1$  is not satisfied, the influence of the weaker driving field on the system needs to be further considered.

The high-order correction effect of the weaker driving field on the system has been observed in experiments by Gustin *et al.* [29]. Although they have given a numerical explanation of the experiment through the Floquet theory, so far no transparent analytical explanation has been given for the asymmetric spectrum that appears in bichromatically driven experiments. Here, the SWPT is used to calculate the effective Hamiltonian of the system and analyze the correction of the system by the weaker field in detail.

The Schrieffer-Wolff transformation  $U_K = e^{-iK(t)}$  is used to get an effective Hamiltonian  $H_{\text{eff}}(t) = U_K^\dagger [H'_1(t) - i\partial_t] U_K$ . The parameter  $K(t)$  is the generator of the Schrieffer-Wolff transformation, i.e.,  $K(t) = \sum_n \lambda^n K_n(t)$ , where  $\lambda$  means the order of the perturbation with the weaker field coupling, and  $K_n(t)$  represents the solution of the generator at the order  $\lambda^n$  [30,31,44,45]. In the interest of brevity, only the conclusion is given:

$$H'_{\text{eff}} = \sum_{j=1,2,3} H'_{\text{eff}}^{(j)}, \quad (5)$$

with

$$H'_{\text{eff}}^{(1)} = \frac{\Omega_2}{2} (R_+ + R_-) + \frac{\delta}{2} R_z, \quad (6a)$$

$$H'_{\text{eff}}^{(2)} = \frac{\Omega_2}{2} \frac{\alpha}{8} R_z, \quad (6b)$$

$$H'_{\text{eff}}^{(3)} = -\frac{\Omega_2}{2} \frac{25\alpha^2}{64} (R_+ + R_-). \quad (6c)$$

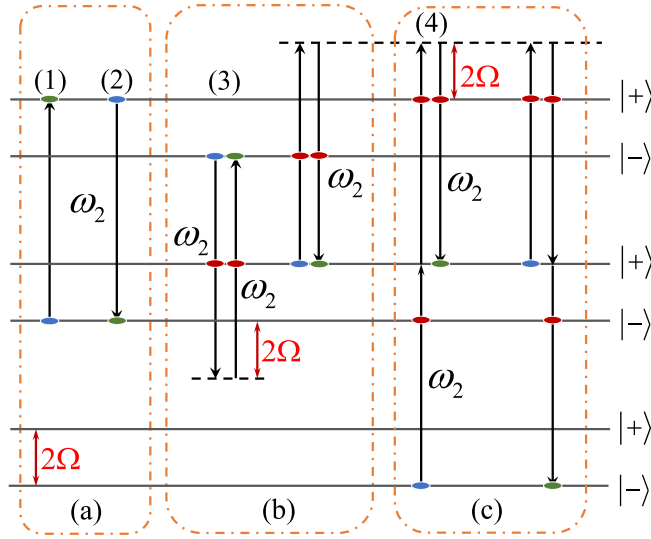


FIG. 2. Multiphoton process in effective Hamiltonian.  $|+\rangle$  and  $|-\rangle$  are the atomic energy levels of the first dressed representation, respectively. Blue ellipse: initial trigger state; red ellipse: intermediate state; green ellipse: final state. Solid arrows indicate absorption or emission of photons of frequency  $\omega_2$ . (a) The single-photon process corresponding to the first-order effective Hamiltonian. (b) The two-photon process corresponding to the second-order effective Hamiltonian. (c) The three-photon process corresponding to the third-order effective Hamiltonian.

In the first dressed representation, the strong driving field splits each atomic energy level equidistantly with energy  $2\Omega$ . The effective Hamiltonian of different orders in Eqs. (6a)–(6c) correspond to multiphoton correction of different orders by the weaker driving field. From these equations it can be found that as the value of  $\alpha$  increases, the correction effects of the weaker driving field on the system, such as two-photon and three-photon processes, cannot be ignored, namely, the influence of the weaker driving field on the system cannot be simply ignored. The specific processes are shown in Fig. 2.

Figure 2(a) depicts the single-photon resonance process corresponding to the first-order effective Hamiltonian (6a), where the operator  $R_+$  means the first dressed atom absorbs a photon of frequency  $\omega_2$  from the dressed state  $|-\rangle$  to  $|+\rangle$ , as shown in channel (1) in Fig. 2(a). The dressed atom can also emit a photon of frequency  $\omega_2$  from another transition channel (2)  $|+\rangle$  to  $|-\rangle$ , corresponding to the second term  $R_-$  in Eq. (6a).

The second-order effective Hamiltonian (6b), corresponding to the two-photon correction of the weaker driving field to the system, which is the energy shift term, also known as the AC stark effect [46,47], is shown in Fig. 2(b). Take channel (3) as an example. The dressed atom transits from the initial state  $|-\rangle$  to the intermediate state  $|+\rangle$  and emits a photon with frequency  $\omega_2$  into the weaker driving field. Since the single photon does not resonate, the dressed atom immediately absorbs a photon of the same frequency  $\omega_2$  and returns to the initial state  $|-\rangle$ . This second-order nonlinear process can also be achieved through another Raman transition in Fig. 2(b), of course.

The three-photon correction of the weaker field to the system is shown as the third-order effective Hamiltonian (6c), corresponding to the third-order nonlinear process in Fig. 2(c). Such as transition (4), the dressed atom absorbs a photon of frequency  $\omega_2$  from the weaker field and undergoes a transition  $|-\rangle \rightarrow |-\rangle$ , and then continues to absorb a photon of frequency  $\omega_2$  to jump to state  $|+\rangle$ . Since the entire cascaded two-photon process is nonresonant, the dressed atom immediately emits a photon of frequency  $\omega_2$  and undergoes transition from state  $|+\rangle$  to state  $|+\rangle$ . This cascaded Raman process with one common transition constitutes a three-photon correction process. This process forms part of the first term in Eq. (6c),  $R_+ = |+\rangle\langle -|$ , which can also be achieved through another channel as shown or other channels not shown in Fig. 2(c). This correction of the system by the three-photon process appears as a saturation effect [48].

In order to investigate the influence on the system when the weaker field coupling strength is strong, the Hamiltonian (5) is diagonalized to enter the second dressed representation. The eigenvalues and eigenstates of this representation are  $\pm\Omega_3$  and  $|+\prime\rangle = s_2|-\rangle + c_2|+\rangle$ ,  $|-\prime\rangle = c_2|-\rangle - s_2|+\rangle$  with  $s_2^2 = 1/2 - \Omega_2^2/32\Omega\Omega_3$  and  $c_2^2 = 1/2 + \Omega_2^2/32\Omega\Omega_3$ , respectively. The second dressed transformation  $U_{d2}$  is introduced,

$$U_{d2} = \begin{bmatrix} c_2 & -s_2 \\ s_2 & c_2 \end{bmatrix}, \quad (7)$$

and the Hamiltonian of the second dressed representation is obtained by  $H''_{AL} = U_{d2}^\dagger H'_{\text{eff}} U_{d2}$ , i.e.,

$$H''_{AL} = \Omega_3 R'_z, \quad (8)$$

with

$$\Omega_3 = \sqrt{\left(\frac{\Omega_2^2}{16\Omega} + \frac{\delta}{2}\right)^2 + \frac{\Omega_2^2}{4} \left(1 - \frac{25\alpha^2}{64}\right)^2}, \quad (9)$$

where  $R'_z = |+\prime\rangle\langle +\prime| - |-\prime\rangle\langle -\prime|$  is the atomic inversion operator and  $\Omega_3$  is a generalized Rabi frequency in this representation. The saturation effect of the Hamiltonian (6c) will affect the secondary splitting of energy levels in the second dressed representation.

### C. Multiphoton correction of spontaneous emission by weaker driving field

The Hamiltonian of the interaction between the atom and the spontaneous emission reservoir in the original representation is

$$H_{AR} = \sum_k g_k (a_k^\dagger \sigma_- e^{i(\omega_k - \omega_1)t} + \text{H.c.}), \quad (10)$$

in which parameter  $g_k$  is the coupling constant of the mode  $k$  in the spontaneous emission reservoir to the atom. Operator  $a_k$  is the annihilation operator for the mode- $k$  photon in the spontaneous emission reservoir.

#### 1. Spontaneous emission process in first dressed representation

After the operator  $\sigma_-$  in the Hamiltonian (10) undergoes the first dressed transformation, the rotation transformation with the frequency of  $2\Omega$ , and the perturbation transformation (i.e.,  $U_1 = U_{d1} U_\Omega U_K$ ), the atomic operator of the third-order

perturbation in the first dressed representation is

$$U_1^\dagger \sigma_- U_1 = \sum_{\substack{j=0,\pm \\ k=0,\dots,\pm 4}} [M_{2k}^{(j)} R_j] e^{2ik\Omega t}, \quad (11)$$

where the coefficient  $M_{2k}^{(j)}$  is the transition weight with third-order perturbation. For specific expressions see Eq. (A2) in Appendix. It is not difficult to conclude from Eq. (11) that with the coupling of the weaker field, the weaker field generates high-order correction to the atomic transition operator of spontaneous emission, so that the corresponding high-order harmonic generated in the dressed representation, and each high-order harmonic split into triplet again. As a result, a richer high-order harmonic spectrum than the familiar Mollow triplet can be obtained.

It can also be seen from Eq. (A2) that the different multiphoton process with a weaker driving field has different effects on the transition weights of the atom in the first dressed representation. Here we take the three peaks of the central band as an example, i.e.,  $k = 0$ , and the detailed expression is

$$M_0^{(0)} R_z + M_0^{(+)} R_+ + M_0^{(-)} R_-, \quad (12)$$

with

$$M_0^{(0)} = 1/2 - \alpha^2/64, \quad (13a)$$

$$M_0^{(+)} = \alpha/4 + 77\alpha^3/1536, \quad (13b)$$

$$M_0^{(-)} = -\alpha/4 + 17\alpha^3/1536. \quad (13c)$$

According to Eq. (12) and Eqs. (13a)–(13c), the weaker driving field has different orders of corrections to the central peak and sidepeaks of the central band. What is more noteworthy is that its first-order corrections  $-\alpha/4$  and  $\alpha/4$  for the peaks on both sides are just the opposite, which is the main factor for the appearance of asymmetric spectra of the system. The detailed analysis is shown in Fig. 3.

Figure 3(a) shows the first-order correction of the weaker driving field to the sidepeaks of the central band, corresponding to the first terms of Eqs. (13b) and (13c), respectively. Take channel (1) as an example. The dressed atom transits from state  $|+\rangle$  to state  $|+\rangle$  and emits a photon with frequency  $\omega_2$  into the weaker driving field. The dressed atom then immediately transits from the intermediate state  $|+\rangle$  to the final state  $|-\rangle$  and emits a photon of frequency  $\omega_1$  due to single-photon nonresonance. This cascaded two-photon process [32] constitutes a part of the third term  $R_- = |-\rangle\langle +|$  in Eq. (12). Similarly, the Raman two-photon processes depicted in channel (2) constitute the first-order correction of the weaker driving field in the second term  $R_+ = |+\rangle\langle -|$  in Eq. (12). The cascaded process and Raman process show that the effect of the weaker driving field on the first-order correction of spontaneous emission is just opposite. This is also the main reason for the unequal population of dressed-state energy levels. The two transition channels in Fig. 3(c) describe the third-order correction of the sidepeaks by the weaker driving field, which will not be described in detail here.

Figure 3(b) describes the second-order correction of the weaker driving field on the central peak of the central band. This process corresponds to the first term  $R_z$  in Eq. (12). Take

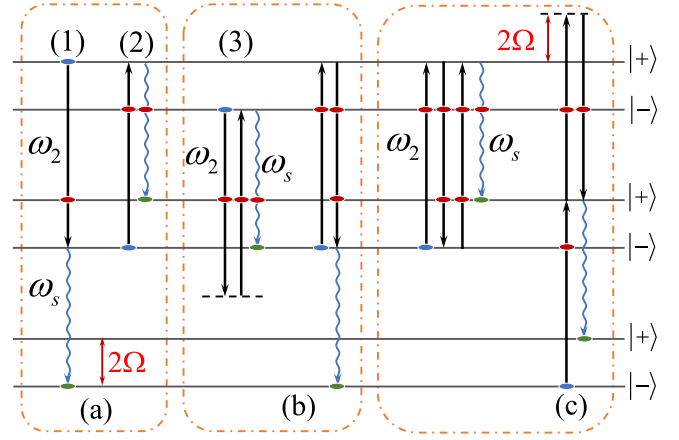


FIG. 3. Multiphoton correction process of the central band of spontaneous emission in the first dressed representation by weaker driving field.  $|+\rangle$  and  $|-\rangle$  are the atomic energy levels of the first dressed representation, respectively. Blue ellipse: initial states; red ellipse: intermediate state; green ellipse: final state. Weaker driving field frequency (solid arrow) is  $\omega_2$ ; emission frequency (wavy arrow)  $\omega_s$  of the central band of the spontaneous emission fluorescence spectrum. (a) First-order correction process, (b) second-order correction process, and (c) third-order correction process.

channel (3) as an example. The dressed atom emits a photon with frequency  $\omega_2$  from state  $|-\rangle$ , and then immediately absorbs a photon with the same frequency  $\omega_2$  coming to the state  $|+\rangle$ . Since the two-photon does not resonate, it immediately emits a photon with frequency  $\omega_1$  to the final state  $|-\rangle$ , completing a transition  $|-\rangle \rightarrow |-\rangle$ . These multiphoton correction processes directly or indirectly affect the system fluorescence spectrum and photon statistical properties.

## 2. Spontaneous emission process in second dressed representation

Equation (11) undergoes a new dressed transformation  $U_{d2}$  into the second dressed representation read by

$$U_{d2}^\dagger U_1^\dagger \sigma_- U_1 U_{d2} = \sum_{\substack{j=0,\pm \\ k=0,\dots,\pm 4}} [\Pi_{2k}^{(j)} R'_j] e^{2ik\Omega t}, \quad (14)$$

in which coefficient  $\Pi_{2k}^{(j)}$  is transition weight with third-order perturbation in second dressed representation. For specific expressions, see Eq. (A3) in Appendix. Take the three peaks of the central band as an example also, that is,  $k = 0$ . The detailed expression is

$$\Pi_0^{(0)} R'_0 + \Pi_0^{(+)} R'_+ + \Pi_0^{(-)} R'_-, \quad (15)$$

where

$$\Pi_0^{(0)} = \left( \frac{1}{2} - \frac{\alpha^2}{64} \right) (c_2^2 - s_2^2) - \frac{47\alpha^3}{768} s_2 c_2, \quad (16a)$$

$$\Pi_0^{(-)} = \left( 1 - \frac{\alpha^2}{32} \right) s_2 c_2 - \frac{\alpha}{4} + \frac{17\alpha^3}{1536} c_2^2 - \frac{77\alpha^3}{1536} s_2^2, \quad (16b)$$

$$\Pi_0^{(+)} = \left( 1 - \frac{\alpha^2}{32} \right) s_2 c_2 + \frac{\alpha}{4} - \frac{17\alpha^3}{1536} s_2^2 + \frac{77\alpha^3}{1536} c_2^2. \quad (16c)$$

From the expressions of  $\Pi_0^{(+)}$  and  $\Pi_0^{(-)}$ , the first-order correction of the weaker driving field is the main factor for the

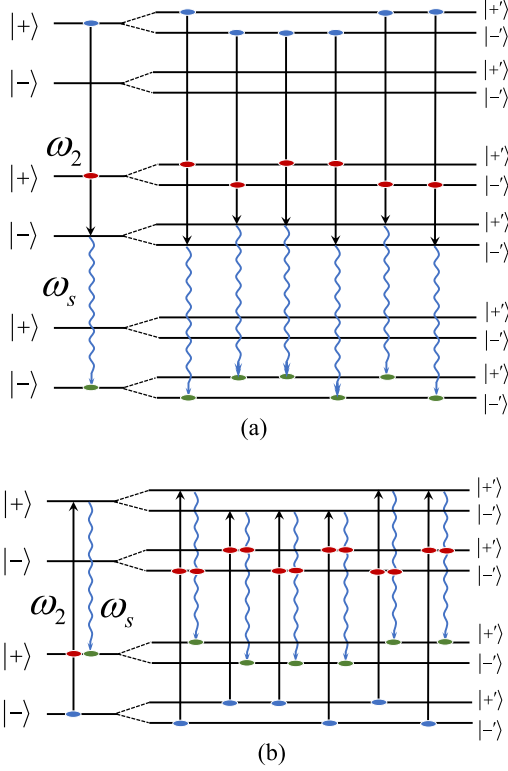


FIG. 4. Two-photon correction of the central band of spontaneous emission in the first dressed representation and the second dressed representation by the weaker driving field.  $|+\rangle$  and  $|-\rangle$  are the atomic energy levels of the first dressed representation, respectively.  $|+\rangle'$  and  $|-\rangle'$  are the atomic energy levels of the second dressed representation, respectively. First dressed representation: (a) cascaded two-photon process; (c) Raman two-photon process. Second dressed representation: (b) six cascaded two-photon processes; (d) six Raman two-photon processes.  $\omega_2$ , weaker driving field frequency (solid arrow);  $\omega_s$  spontaneous emission fluorescence frequency (wavy arrow). Blue ellipse: initial states; red ellipse: intermediate state; green ellipse: final states.

asymmetry of the sidepeaks in the central band. Of course, as the strength of the weak driving field increases, higher-order effects will gradually appear.

As analyzed in the Sec. II C 1, the cascaded two-photon process described in Fig. 4(a) is a first-order correction process of one of the sidepeaks in the central band in the first dressed representation by the weaker driving field. The transition operators  $R_z$ ,  $R_+$ , and  $R_-$  in Eq. (12) are expanded in the second dressed representation, then one cascaded two-photon process in the first dressed representation is decomposed into six cascaded two-photon processes in the second dressed representation, as shown in Fig. 4(b). Figures 4(c) and 4(d) respectively correspond to the Raman two-photon correction process of the sidepeaks of the central band in two dressed representations by the weaker driving field. Based on these, the first-order correction of the central peak of the central band by the weaker driving field has an important effect in both dressed representations. As the strength of the weaker driving field increases, the influence of higher-order corrections gradually emerges, which is also the main factor of the

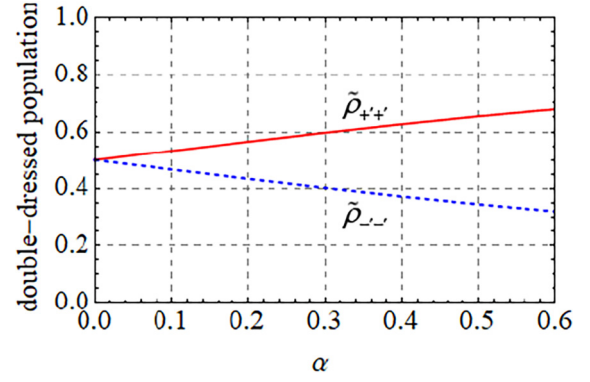


FIG. 5. The steady-state population distribution of the second dressed representation.  $\tilde{\rho}_{++}'$  (red solid line),  $\tilde{\rho}_{--}'$  (blue dotted line).

fluorescence spectrum asymmetry discussed later. The process of the first-order correction of the high-order sidebands by the weaker driving field is discussed in Appendix.

#### D. Fluorescence spectrum

Under conditions of the atomic radiation rate  $\gamma_{0,\pm} \ll 2\Omega$  and secular approximation, Eqs. (8), (10), and (14) are substituted into the Lindblad master equation [49,50] in the second dressed representation, i.e.,

$$\dot{\tilde{\rho}} = -i[H_{AL}'', \tilde{\rho}] + \sum_{j=0,\pm} \frac{\gamma_j}{2} \mathcal{L}[R_j']\tilde{\rho}, \quad (17)$$

where  $\mathcal{L}[c]\tilde{\rho} = 2c\tilde{\rho}c^\dagger - c^\dagger c\tilde{\rho} - \tilde{\rho}c^\dagger c$ , and the parameter  $\gamma_j$  is the atomic radiation rate in the second dressed representation. The specific expression is

$$\gamma_j = \gamma \sum_{k=0,\pm 1,\dots,\pm 4} [\Pi_{2k}^{(j)}]^2 \quad (j = 0, \pm). \quad (18)$$

From the master equation (17) the time evolution of the population of the second dressed representation can be found as

$$\begin{aligned} \frac{d}{dt} \tilde{\rho}_{++}' &= \gamma_+ \tilde{\rho}_{--}' - \gamma_- \tilde{\rho}_{++}', \\ \frac{d}{dt} \tilde{\rho}_{--}' &= -\gamma_+ \tilde{\rho}_{--}' + \gamma_- \tilde{\rho}_{++}'. \end{aligned} \quad (19)$$

The steady-state solution of Eq. (19) is easily obtained by

$$\tilde{\rho}_{++}' = \frac{\gamma_+}{\gamma_+ + \gamma_-}, \quad \tilde{\rho}_{--}' = \frac{\gamma_-}{\gamma_+ + \gamma_-}. \quad (20)$$

According to Eq. (20), it can be found that the population distribution of the upper and lower energy levels of the second dressed representation is related to the transition rates  $\gamma_+$  and  $\gamma_-$  of the secondary dressed atom, respectively. From the analysis in the Sec. II C, it can be seen that the multiphoton correction of different orders of spontaneous emission by the weaker driving field makes  $\gamma_+$  and  $\gamma_-$  unequal, which leads to the unequal population distribution of the upper and lower energy levels in the second dressed representation.

As shown in Fig. 5, when the coupling strength of the weaker driving field is large, the populations of the upper and lower energy levels are obviously unequal. When the intensity of the weaker driving field is much smaller than the strong

one, the effect of the weaker field can be ignored according to the rotating-wave approximation, and the population distribution of the upper and lower energy levels of the second dressed representation is equal. This matches what is shown in Fig. 5, when  $\alpha \sim 0.02$ ,  $\tilde{\rho}_{++'} \approx \tilde{\rho}_{--'} = 0.5$ , so the fluorescence spectrum has symmetry. This result is consistent with the analytical interpretation of Ficek and Freedhoff [18]. With the intensity of the weaker driving field strengthened, that is, with the increase of  $\alpha$ , the correction by the weaker field on the system and spontaneous emission becomes stronger and stronger, and its accompanying multiphoton process makes the population distribution of the upper and lower energy levels of the second dressed representation no longer equal, with the increase of  $\alpha$  the difference between the  $\tilde{\rho}_{++'}$  and  $\tilde{\rho}_{--'}$  increased also. As shown in Fig. 5, when  $\alpha > 0.1$ , there is a clear difference in the values of  $|+' \rangle$  and  $|-'\rangle$ . Therefore it can be preliminarily judged that the incoherent spectrum of the system has asymmetry. This conclusion is inconsistent with the analytically calculated symmetric spectrum mentioned by Ficek and Freedhoff [18]. This is because they only considered the correction of the system by the weaker driving field but ignored its multiphoton correction of spontaneous emission. Next, the characteristics of the fluorescence spectrum are analyzed in detail.

The incoherent resonance fluorescence spectrum of the atom can be expressed by the term of the two-time correlation function of the atomic operators [51],

$$S_{\text{in}}(\omega) = \text{Re} \int_0^{\infty} d\tau e^{-i\omega\tau} \lim_{t \rightarrow \infty} \langle \delta\sigma_+(t+\tau)\delta\sigma_-(t) \rangle, \quad (21)$$

where  $\delta\sigma_{\pm} = \sigma_{\pm} - \langle \sigma_{\pm} \rangle$ . Applying the master equation (17), the average values of dressed atomic operators satisfy the following set of equations:

$$\begin{aligned} \frac{d}{dt} \langle R_+ \rangle &= (2i\Omega_3 - \gamma_c) \langle R_+ \rangle, \\ \frac{d}{dt} \langle R_- \rangle &= (-2i\Omega_3 - \gamma_c) \langle R_- \rangle, \end{aligned} \quad (22)$$

in which relaxation coefficient  $\gamma_c$  is defined by  $\gamma_c = \frac{1}{2}(4\gamma_0 + \gamma_+ + \gamma_-)$ . Applying the quantum regression theory, we can get the analytical solution of the steady-state incoherent spectrum

$$\begin{aligned} S_{\text{in}}(\omega) &= \sum_{k=0, \pm 1, \dots, \pm 4} \left[ 4\Pi_{2k}^{(0)^2} \frac{\rho_{++'}\rho_{--'}\gamma_1}{(\omega + 2k\Omega)^2 + \gamma_1^2} \right. \\ &+ \Pi_{2k}^{(-)^2} \rho_{++'} \frac{\gamma_c}{(\omega - 2k\Omega - 2\Omega_3)^2 + \gamma_c^2} \\ &\left. + \Pi_{2k}^{(+)^2} \rho_{--'} \frac{\gamma_c}{(\omega + 2k\Omega + 2\Omega_3)^2 + \gamma_c^2} \right], \end{aligned} \quad (23)$$

where  $\gamma_1 = (\gamma_+ + \gamma_-)$ . Our analytical solution is consistent with the numerical results of Rudolph *et al.* [20] and the experimental results of Gustin *et al.* [29]. Meanwhile, when the coupling strength  $\Omega_2$  of the weaker driving field is small, our analytical solution is consistent with that of Ficek and Freedhoff [18].

The fluorescence spectrum of this case is more complex than that driven by a monochromatic field. When there is only

one strong driving field, the fluorescence spectrum is a standard Mollow triplet structure, and the frequency of each peak is  $\{\omega, \omega \pm 2\Omega\}$ , corresponding to Hamiltonian (3). Due to the multiphoton correction of the nonresonance weaker driving field, the Mollow triplet band structures are corrected into a multipeak structure, and the frequency of each peak is  $\{\omega, \omega \pm 2k\Omega\} (k = 0, \dots, 4)$ , corresponding to Hamiltonian (5). Each peak splits again into three smaller peaks with a frequency interval of  $2\Omega_3$ , corresponding to Hamiltonian (8), as shown in Figs. 6(a)–6(c). When  $\delta = 0$ , with the increase of intensity of the weaker driving field, the asymmetry of the spectrum becomes more and more obvious. This solution is consistent with the numerical results Ref. [18]. According to the spontaneous emission atomic transition operator Eq. (11) and the incoherent fluorescence Eq. (23) in the second dressed representation discussed above, we find that the intensity of each peak largely depends on population distribution  $\tilde{\rho}_{\pm\pm'}$  and transition weight  $\Pi_{2k}^{(0,\pm)}$  ( $k = 0, \pm 1, \dots, \pm 4$ ). It can be seen that the weaker field is very important for the modification of the system and the spontaneous emission. Equation (23) also shows the intensity of the central-band triplet is proportional to  $4\Pi_0^{(0)^2} \rho_{++'}\rho_{--'}$ ,  $\Pi_0^{(-)^2} \rho_{++'}$  and  $\Pi_0^{(+)^2} \rho_{--'}$ , respectively; when  $\alpha = 0.4$ , it is not difficult to get  $\Pi_0^{(-)^2} \rho_{++'} \sim 0.098$  and  $\Pi_0^{(+)^2} \rho_{--'} \sim 0.133$ . This ratio is basically consistent with the ratio of the most obvious high-frequency peak to the low-frequency peak in the central band shown in Fig. 6(b).

Additionally, when  $\alpha$  is small, the central peak of the central band is barely visible. As the value of  $\alpha$  increases, the intensity of the three peaks at frequencies  $\omega = \{\omega_1 \pm 2k\Omega\}$ , ( $k = 2, 3, 4$ ) will become stronger and stronger, and the peak at frequency  $\omega_1$  will emerge. Just as shown in Figs. 6(a), 6(b) and 6(c), when  $\alpha = 0.2$ , the central peak at  $\omega_1$  does not appear; when  $\alpha = 0.4$  the central peak at  $\omega_1$  emerges, and when  $\alpha = 0.6$  the central peak is already very obvious. What needs to be emphasized here is that if only the second-order modification is considered, according to the expression of effective Hamiltonian Eq. (6), in conditions of  $2\Omega = 40$ ,  $\alpha = 0.4$ ,  $\delta = 0.4$ , the central peak of the central band is completely suppressed. And the effective Hamiltonian expression of the system is consistent with the effective Hamiltonian mentioned by Wang *et al.* in Ref. [52] on spin locking. Therefore the method of using SWPT to deal with the Hamiltonian of the similar system is also meaningful for the realization of spin locking.

Based on the fact that  $\alpha \sim 0.5$  in this paper, the peaks of the frequencies at  $\omega = \{\omega_1 \pm 4\Omega, \omega_1 \pm 6\Omega, \omega_1 \pm 8\Omega\}$  in the spectra are not prominent, so the follow-up discussion will mainly focus on first-order harmonics ( $\omega = \omega_1 \pm 2\Omega$ ). Corresponding to nine kinds of spontaneous emission of atoms in the second dressed representation,

$$\sigma_- \rightarrow R'_{\text{Ff}} + R'_{\text{Fr}} + R'_{\text{Ft}} + R'_{\text{Rf}} + R'_{\text{Rr}} + R'_{\text{Rt}} + R'_{\text{Tf}} + R'_{\text{Tr}} + R'_{\text{Tt}}, \quad (24)$$

in which the index ‘‘F’’, ‘‘T’’, ‘‘R’’ represents the low-frequency sideband, high-frequency sideband, and the central band, and ‘‘f’’, ‘‘r’’, ‘‘t’’ represent the left, middle and right peaks of the three bands above. In the next section we present the filtered photon statistical properties of resonance fluorescence considered under the condition of two-photon resonance.

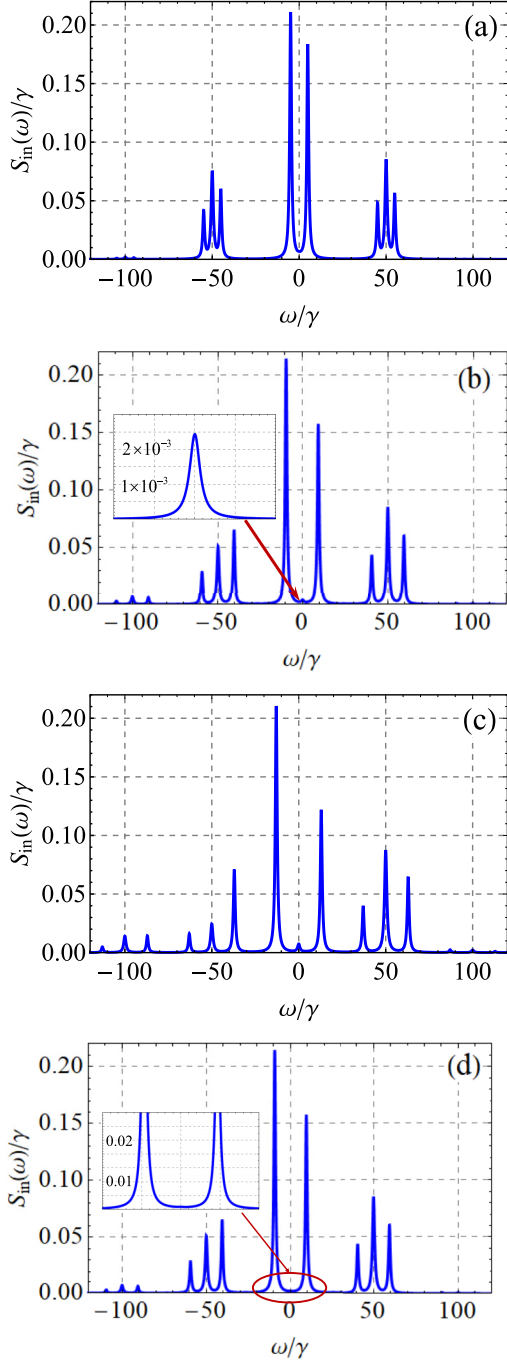


FIG. 6. The incoherent fluorescence spectrum for  $2\Omega = 50\gamma$ , and different  $\alpha = \Omega_2/\Omega_1$  and  $\delta$ : (a)  $\alpha = 0.2, \delta = 0$ ; (b)  $\alpha = 0.4, \delta = 0$ ; (c)  $\alpha = 0.6, \delta = 0$ ; (d)  $\alpha = 0.4, \delta = 0.5$ .

### III. TEMPORAL INTENSITY CORRELATIONS

Having discussed the properties of the incoherent fluorescence spectrum of the two-level atom which is driven by a bichromatic field with different frequencies, we continue with the characteristic of the frequency-resolved photon correlation between the individual components of this incoherent spectrum, which have been researched by Ben-Aryeh *et al.* [41]. However, since they did not consider the correction of the spontaneous emission operator with the weaker field coupling,

the population distribution of the second dressed state is equal. Through the detailed analytical calculation in Sec. II, with the coupling of the weaker field and the increase of the intensity, the upper and lower energy-level population distribution of the second dressed representation are no longer equal, which makes the spectrum appear obvious asymmetry. Therefore it can be deduced that the time-frequency resolved correlated signals between different components in the incoherent fluorescence spectrum also exhibit asymmetry.

Two single-mode cavities with frequencies  $\omega_a$  and  $\omega_b$  are weakly coupled to a quantum emitter to simulate the Lorentzian filter [42]. The coupling strength of two cavities is  $g_1$  and  $g_2$ , respectively. The dissipation coefficients of two cavities are  $\kappa_a, \kappa_b$ , respectively. In order to reveal the photon statistical characteristics of the quantum filter system more intuitively,  $\kappa_a = \kappa_b = \kappa$  and  $g_1 = g_2 = g$  are taken without loss of generality. Meanwhile, the filter system satisfies the condition  $\sqrt{\kappa\gamma} \gg \{g_1, g_2\}$  [42], so that the quantum emitter is weakly coupled to two filtering cavities, and the back action of the cavity to the atom is negligible.

So far, the whole quantum filtering system consists of two parts: a quantum emitter which is modeled by the system mentioned in Sec. II, and two single-mode filtering cavities. The probability to detect one photon at time  $t$  followed by another photon at time  $(t + \tau)$  is proportional to the normalized second-order correlation function between modes  $a$  and  $b$ ,

$$g^2(a, b, \tau) = \frac{\langle a^\dagger(t)b^\dagger(t+\tau)b(t+\tau)a(t) \rangle}{\langle a^\dagger(t)a(t) \rangle \langle b^\dagger(t+\tau)b(t+\tau) \rangle} = \frac{G^{(2)}(a, b, \tau)}{G_a^{(1)}G_b^{(1)}}, \quad (25)$$

in which  $G^{(2)}(a, b, \tau)$  is the un-normalized second-order correlation function between two modes, and  $G_a^{(1)}$  and  $G_b^{(1)}$  are the first-order correlation functions in two modes, respectively. The master equation of the time evolution of density operator  $\rho$  in the dipole approximation and rotating-wave approximation [51] are written as

$$\dot{\rho} = -i[H_s, \rho] + \mathcal{L}_A\rho + \mathcal{L}_C\rho, \quad (26)$$

where the last two terms denote the dissipation of the atom and the cavity, respectively. The Hamiltonian of the quantum filtering system is

$$\begin{aligned} H_s = & \frac{1}{2}\omega_0\sigma_z + \omega_a a^\dagger a + \omega_b b^\dagger b \\ & + \Omega_1(\sigma_+ e^{-i\omega_1 t} + \text{H.c.}) \\ & + \Omega_2(\sigma_+ e^{-i\omega_2 t} + \text{H.c.}) \\ & + g(a^\dagger \sigma_- + \text{H.c.}) + g(b^\dagger \sigma_- + \text{H.c.}). \end{aligned} \quad (27)$$

After unitary transformation  $U = U_{d1}U_\Omega U_K U_{d2}$ , the Hamiltonian of the quantum filtering system in the second dressed representation can be expressed as

$$\begin{aligned} H'_s = & \Omega_3 R'_0 + \Delta_a a^\dagger a + \Delta_b b^\dagger b \\ & + g \sum_{\substack{\beta=0,\pm \\ k=0,\pm 1}} (a^\dagger \Pi_{2k}^{(\beta)} R'_\beta e^{2ik\Omega t} + \text{H.c.}) \\ & + g \sum_{\substack{m=0,\pm \\ l=0,\pm 1}} (b^\dagger \Pi_{2l}^{(m)} R'_m e^{2il\Omega t} + \text{H.c.}), \end{aligned} \quad (28)$$

where  $\Delta_a = \omega_a - \omega_1$  and  $\Delta_b = \omega_b - \omega_1$  are the detuning of frequency of two filtering cavities and frequency of the driving field, respectively. With the different value of the coefficients  $k, \beta, l, m$ , two single-mode filter cavities target different spectral filtering, which will be discussed below.

### A. Complete frequency selection

We suppose that each filter cavity is placed in front of one spectral component, having a bandwidth  $\kappa$  such that  $\Omega_1 > \Omega_2 > \Omega_3 > \kappa$ , and  $\kappa \gg \gamma \gg g$ . The first inequality implies that each filter selects only one particular component of the spectra. Since there are no coherent terms to contribute to the signal, it can be completely described in terms of the population [41]. The second inequality shows that each target spectral line can be completely covered by the corresponding filter. Next, two methods will be applied to analyze photon statistics between different spectral components. First, by calculating the correlation moment and applying the quantum regression theorem and Laplace transform to obtain the normalized two-mode second-order correlation function. Then, under the condition of  $\kappa \gg \gamma \gg g$  [53] and short-time detection, the short-delay signal characteristics of two-photon correlation are analyzed by using the conditional quantum state and wave function [54,55].

For the convenience of subsequent discussion, the nine peak frequencies in the spectra can be marked as

$$\begin{aligned} \omega_{Ff} &= \omega_1 - 2\Omega - 2\Omega_3, & \omega_{Ft} &= \omega_1 - 2\Omega, \\ \omega_{Ft} &= \omega_1 - 2\Omega + 2\Omega_3, & \omega_{Rf} &= \omega_1 - 2\Omega_3, \\ \omega_{Rt} &= \omega_1 + 2\Omega_3, & \omega_{Tf} &= \omega_1 + 2\Omega - 2\Omega_3, \\ \omega_{Tr} &= \omega_1 + 2\Omega, & \omega_{Tt} &= \omega_1 + 2\Omega + 2\Omega_3, \\ \omega_{Rr} &= \omega_1, \end{aligned} \quad (29)$$

where  $\omega_{Ft}$  is the high-frequency component of the triplet centered at the low-frequency component of the original Mollow triplet. Next, two typical examples are used to further investigate the influence of the nonlinear multiphoton effect by the weaker driving field on the photon statistical properties of the system.

#### 1. Filtering between different sidepeaks

The  $a$ -mode filter is centered at frequency  $\omega_{Ff}$  and the  $b$ -mode filter is centered at frequency  $\omega_{Tt}$ , as shown in Fig. 8(a). In this situation the specific form of the Hamiltonian (28) in the second dressed representation is

$$\begin{aligned} H_s'' &= \Omega_3 R'_0 + (\Delta_a + 2\Omega)a^\dagger a + (\Delta_b - 2\Omega)b^\dagger b \\ &+ g\Pi_2^{(+)}(a^\dagger R'_+ + \text{H.c.}) + g\Pi_{-2}^{(-)}(b^\dagger R'_- + \text{H.c.}). \end{aligned} \quad (30)$$

The master equation of the system, including the filtering process, is

$$\dot{\rho} = -i[H_s'', \rho] + \frac{\kappa}{2}(\mathcal{L}_a \rho + \mathcal{L}_b \rho) + \sum_{i=0, \pm} \frac{\gamma_i}{2} \mathcal{L}[R'_i] \rho. \quad (31)$$

According to the master equation in the second dressed representation, we derive the equation of motion of the two-mode atom-photon correlation moment of the type  $\langle a_\alpha^{\dagger m} b_\beta^{\dagger n} b_\beta^p a_\alpha^q R'_{st\lambda} \rangle$  ( $\alpha = Ff, \beta = Tt$ , and  $R'_{st\lambda}$  is the transition

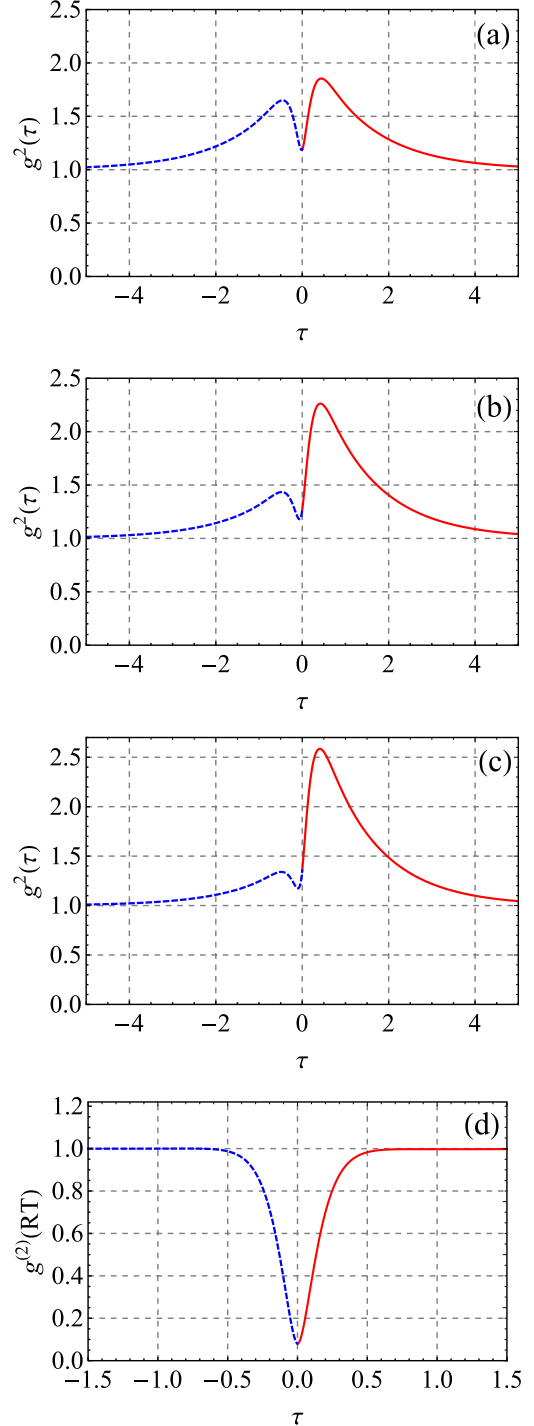


FIG. 7. Time-frequency resolved correlated signals between different components in the fluorescence spectra. The parameters  $\Omega = 40\gamma$ ,  $\kappa = 8\gamma$ ,  $\delta_a = -\delta_b = 2\gamma$ ; (a):  $\alpha = 0.1$ , (c):  $\alpha = 0.6$ , (b) and (d):  $\alpha = 0.4$ . The red solid line presents the normalized  $g^{(2)}(b, a, \tau)$ , the blue dotted line present the normalized  $g^{(2)}(a, b, \tau)$ . (a), (b), and (c)  $a$ -mode filter centered at frequency  $\omega_{Ff}$  and  $b$ -mode filter centered at frequency  $\omega_{Tt}$ ; (d)  $a$ -mode filter centered at frequency  $\omega_{Rr}$  and  $b$ -mode filter centered at frequency  $\omega_{Tt}$ .

operator in the second dressed state,  $s, t \in \{+, -\}$ ,

$$\frac{d}{dt} \langle (a_\alpha^{\dagger m} b_\beta^{\dagger n} b_\beta^p a_\alpha^q R'_{st\lambda})(t) \rangle = \text{Tr} \left( a_\alpha^{\dagger m} b_\beta^{\dagger n} b_\beta^p a_\alpha^q R'_{st\lambda} \frac{d\tilde{\rho}}{dt} \right). \quad (32)$$

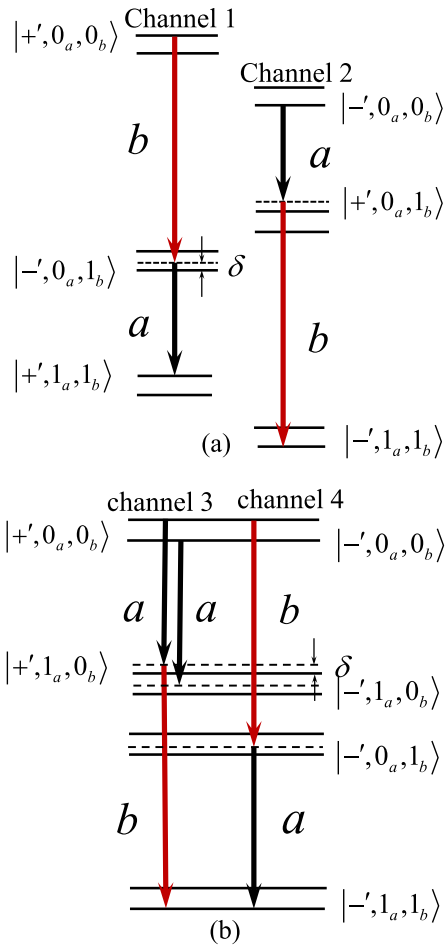


FIG. 8. Transition paths and time ordering of two-photon resonant cascaded emission of photon pair (a,b), in which channel 1 and channel 2 are independent time-ordering channels, and channel 3 and channel 4 display interference involving a common initial dressed state and a final dressed state. Black and red arrows represent the photon emissions in modes  $a$  and  $b$ , respectively.

Then the single-mode second-order correlation of two optical cavities can be obtained by

$$\begin{aligned} \frac{d}{dt} \langle b^\dagger(\tau)b(\tau) \rangle &= -ig\Pi_{-2}^{(-)} (\langle b^\dagger(\tau)R'_-(\tau) \rangle - \langle b(\tau)R'_+(\tau) \rangle) \\ &\quad - \kappa \langle b^\dagger(\tau)b(\tau) \rangle, \\ \frac{d}{dt} \langle a^\dagger(\tau)a(\tau) \rangle &= -ig\Pi_{-2}^{(+)} (\langle a^\dagger(\tau)R'_+(\tau) \rangle - \langle a(\tau)R'_-(\tau) \rangle) \\ &\quad - \kappa \langle a^\dagger(\tau)a(\tau) \rangle. \end{aligned} \quad (33)$$

In this way the filtered intensity of the target spectrum can be obtained by

$$\begin{aligned} \langle a^\dagger a \rangle_s &= \frac{g^2 \Pi_{-2}^{(+)} (\kappa + 2\gamma_c) \rho_{--}}{\kappa [(\frac{\kappa}{2} + \gamma_c)^2 + \delta_a^2]}, \\ \langle b^\dagger b \rangle_s &= \frac{g^2 \Pi_{-2}^{(-)} (\kappa + 2\gamma_c) \rho_{++}}{\kappa [(\frac{\kappa}{2} + \gamma_c)^2 + \delta_b^2]}, \end{aligned} \quad (34)$$

in which  $\delta_a = \Delta_a + 2\Omega + 2\Omega_3$  and  $\delta_b = \Delta_b - 2\Omega - 2\Omega_3$  are the detuning of two filters and the target line, respectively.

Applying the quantum regression theorem and Laplace transform, the normalized two-mode second-order correlation functions  $g^{(2)}(a, b, \tau)$  and  $g^{(2)}(b, a, \tau)$  can be gotten according to Eq. (33), as shown in Fig. 7(b). In addition to the bunching behavior displayed in the figure, the other obvious feature is the significant asymmetry in the time ordering of the two-mode second-order correlation function, which differs significantly from the correlation signal of the familiar Mollow spectrum [56].

Since the correlation moment cannot give a clear physical picture, for this reason, under the condition of  $\kappa \gg \gamma$  and short-time detection, the wave function and the conditional quantum state are used to explain the system analytically. The un-normalized two-mode and second-order correlation function for detecting one  $a$ -mode photon at time  $t$  and followed by detecting one  $b$ -mode photon at time  $(t + \tau)$  can be expressed as

$$G^{(2)}(a, b, \tau) = \text{Tr}[b^\dagger b \rho_r(\tau)], \quad (35)$$

in which  $\rho_r(\tau) = [a^\dagger \rho(\infty) a]_\tau$  is the conditional quantum state of the quantum filter system after detecting one  $a$ -mode photon, which can be expressed as  $\rho_r(\tau) = e^{-iHt} [a(0) \rho(\infty) a^\dagger(0)]$ . This means that if a cavity preselects an  $a$ -mode photon, then only the possibility of another filter cavity producing a  $b$ -mode photon needs to be considered. The system state function is expanded as follows:

$$\begin{aligned} |\psi_{+'}(t)\rangle &= |+', 0_a, 0_b\rangle + B_{1-'} |-', 0_a, 1_b\rangle \\ &\quad + A_{2+'} |+', 1_a, 1_b\rangle, \\ |\psi_{-'}(t)\rangle &= |-', 0_a, 0_b\rangle + A_{1+'} |+', 1_a, 0_b\rangle \\ &\quad + B_{2-'} |-', 1_a, 1_b\rangle, \end{aligned} \quad (36)$$

where  $B_{1-}$  and  $A_{2+}$  denote the conditional probability amplitudes for successive emission of  $b$ -mode photons and  $a$ -mode photons from the dressed atom in the second dressed representation  $|+'\rangle$  to  $|+\rangle$ , corresponding to channel 1 in Fig. 8(a). This is the reverse timing channel, that is, the detection ordering is opposite to the emission ordering. Channel 2 is a positive timing channel, that is, the emission ordering is the same as the detection ordering. By substituting the Hamiltonian (36) into the Schrödinger equation, a steady-state solution for the conditional probability magnitude can be obtained by

$$\begin{aligned} A_{1+} &= \frac{ig\Pi_{-2}^{(+)}}{\frac{\kappa}{2} + i\delta_a}, \quad B_{1-} = \frac{-ig\Pi_{-2}^{(-)}}{\frac{\kappa}{2} + i\delta_b}, \\ B_{2-} &= \frac{g^2 \Pi_{-2}^{(-)} \Pi_{-2}^{(+)}}{[\frac{\kappa}{2} + i(\delta_b + \delta_a)] (\frac{\kappa}{2} + i\delta_a)}, \\ A_{2+} &= \frac{g^2 \Pi_{-2}^{(-)} \Pi_{-2}^{(+)}}{[\frac{\kappa}{2} + i(\delta_b + \delta_a)] (\frac{\kappa}{2} + i\delta_b)}. \end{aligned} \quad (37)$$

Because the filter system satisfies the two-photon resonance  $\delta_a + \delta_b = 0$ , the single-mode intensities of the two filter

cavities are

$$\begin{aligned} \langle a^\dagger a \rangle_s &= \frac{g^2 \Pi_2^{(+)^2} \rho_{-'-'}}{\left(\frac{\kappa}{2}\right)^2 + \delta_a^2}, \\ \langle b^\dagger b \rangle_s &= \frac{g^2 \Pi_2^{(-)^2} \rho_{+''}}{\left(\frac{\kappa}{2}\right)^2 + \delta_b^2}. \end{aligned} \quad (38)$$

This conclusion is consistent with Eq. (34), which is solved by the equation of the correlation moment in case the dissipation of the atom is ignored. It can be seen that under the condition of short-delay detection, the results of the two methods can be in good agreement. Then the initial value of the density operator of the conditional quantum state can be expressed as

$$\begin{aligned} \rho_{r,a}(0) &= \rho_{+''} |A_{2+''}|^2 |+'', 0_a, 1_b\rangle \langle+'', 0_a, 1_b| \\ &+ \rho_{-'''} |A_{2+''}|^2 |+'', 0_a, 0_b\rangle \langle+'', 0_a, 0_b| + B_{2-'''} |-'', 0_a, 1_b\rangle \\ &\times (A_{2+''}^* \langle+'', 0_a, 0_b| + B_{2-'''}^* \langle-'', 0_a, 1_b|). \end{aligned} \quad (39)$$

Equation (39) shows that after the  $a$ -mode photon is detected, the conditional quantum state for the collapse of the quantum filter system is the  $a$ -mode vacuum state. Then we focus on the evolution of the second term  $|+'', 0_a, 0_b\rangle$  in Eq. (39) to produce a  $b$ -mode photon,

$$|\psi_{+'''}^{\prime}(t)\rangle = |+'', 0_a, 0_b\rangle + B_{1-'''}^{\prime}(t) |-'', 0_a, 1_b\rangle, \quad (40)$$

in which  $B_{1-'''}^{\prime}(t)$  is the probability amplitude of a  $b$ -mode photon emitted by the reverse timing channel 1 in Fig. 8(a). Substitute Eq. (30) and Eq. (40) into Schrödinger's equation to get  $B_{1-'''}^{\prime}(t)$ , and its concrete form is  $B_{1-'''}^{\prime}(t) = -g \Pi_{-2}^{(-)^2} [1 - e^{-(\frac{\kappa}{2} + i\delta_b)t}] / (\frac{\kappa}{2} + i\delta_b)$ . Now, the evolution of the conditional quantum state can be written as

$$\begin{aligned} \rho_{r,a}(\tau) &= \rho_{+'''} |C_1(\tau)|^2 |+'', 0_a, 1_b\rangle \langle+'', 0_a, 1_b| \\ &+ \rho_{-'''} (|+'', 0_a, 0_b\rangle + C_2(\tau) |-'', 0_a, 1_b\rangle) \\ &\times (\langle+'', 0_a, 0_b| + C_2^*(\tau) \langle-'', 0_a, 1_b|), \end{aligned} \quad (41)$$

with

$$\begin{aligned} C_1(\tau) &= \frac{g^2 \Pi_2^{(+)^2} \Pi_{-2}^{(-)^2}}{\frac{\kappa}{2} + i\delta_b} \frac{e^{-(\frac{\kappa}{2} + i\delta_b)\tau}}{\kappa + i(\delta_a + \delta_b)}, \\ C_2(\tau) &= \frac{g^2 \Pi_2^{(+)^2} \Pi_{-2}^{(-)^2}}{\left(\frac{\kappa}{2} + i\delta_a\right)\left(\frac{\kappa}{2} + i\delta_b\right)} \left[ (1 - e^{-(\frac{\kappa}{2} + i\delta_b)\tau}) \right. \\ &\left. + \frac{\left(\frac{\kappa}{2} + i\delta_b\right) e^{-(\frac{\kappa}{2} + i\delta_b)\tau}}{\kappa + i(\delta_a + \delta_b)} \right]. \end{aligned} \quad (42)$$

The un-normalized two-mode correlation function can be expressed by

$$G^{(2)}(a, b, \tau) = \rho_{+'''} |C_1(\tau)|^2 + \rho_{-'''} |C_2(\tau)|^2. \quad (43)$$

The un-normalized correlation function is the incoherent superposition of the emitted photon intensities of positive-time-ordering and reverse-time-ordering channels. However, Eq. (39) shows that the second dressed atom is collapsed according to channel 2, which is a channel of positive time ordering, and the information of the reverse-time-ordering channel 1 is not intuitively reflected. It can be seen from Eq. (39) that the dressed atom is more likely to be trapped in

the positive-time-ordering channel, which is also the preferred channel for the filter detection system. The normalized two-mode and second-order correlation function is

$$\begin{aligned} g^{(2)}(a, b, \tau) &= \frac{1}{\rho_{-'''} \kappa^2 + (\delta_a + \delta_b)^2} e^{-\kappa\tau} \\ &+ \frac{1}{\rho_{+'''}} \left| 1 - \frac{\left(\frac{\kappa}{2} + i\delta_a\right) e^{-(\frac{\kappa}{2} + i\delta_b)\tau}}{\kappa + i(\delta_a + \delta_b)} \right|^2. \end{aligned} \quad (44)$$

If the filter detects one  $b$ -mode photon at time  $t$  and is followed by detection of one  $a$ -mode photon at time  $(t + \tau)$ , the density operator of the conditional quantum state reads

$$\begin{aligned} \rho_{r,b}(\tau) &= \rho_{+'''} (|-'', 0_a, 0_b\rangle + C_1'(\tau) |+'', 1_a, 0_b\rangle) \\ &\times (\langle-'', 0_a, 0_b| + C_1'^*(\tau) \langle+'', 1_a, 0_b|) \\ &+ \rho_{-'''} |C_2'(\tau)|^2 |-'', 1_a, 0_b\rangle \langle-'', 1_a, 0_b|, \end{aligned} \quad (45)$$

where the conditional time ordering transition amplitudes are given by

$$\begin{aligned} C_1'(\tau) &= \frac{g^2 \Pi_2^{(+)^2} \Pi_{-2}^{(-)^2}}{\left(\frac{\kappa}{2} + i\delta_a\right)\left(\frac{\kappa}{2} + i\delta_b\right)} \left[ (1 - e^{-(\frac{\kappa}{2} + i\delta_a)\tau}) \right. \\ &\left. + \frac{\left(\frac{\kappa}{2} + i\delta_a\right) e^{-(\frac{\kappa}{2} + i\delta_a)\tau}}{\kappa + i(\delta_a + \delta_b)} \right] \\ C_2'(\tau) &= \frac{g^2 \Pi_2^{(+)^2} \Pi_{-2}^{(-)^2}}{\frac{\kappa}{2} + i\delta_a} \frac{e^{-(\frac{\kappa}{2} + i\delta_a)\tau}}{\kappa + i(\delta_a + \delta_b)}. \end{aligned} \quad (46)$$

The two-mode correlation can be expressed as

$$G^{(2)}(b, a, \tau) = \rho_{+'''} |C_1'(\tau)|^2 + \rho_{-'''} |C_2'(\tau)|^2. \quad (47)$$

The normalized two-mode and second-order correlation function can be written by

$$\begin{aligned} g^{(2)}(b, a, \tau) &= \frac{1}{\rho_{-'''}} \left| 1 - \frac{\left(\frac{\kappa}{2} + i\delta_b\right) e^{-(\frac{\kappa}{2} + i\delta_a)\tau}}{\kappa + i(\delta_a + \delta_b)} \right|^2 \\ &+ \frac{1}{\rho_{+'''} \kappa^2 + (\delta_a + \delta_b)^2} e^{-\kappa\tau}. \end{aligned} \quad (48)$$

The quantum filtering system preferentially selects the information of the positive-time-ordering channel (1) with the same ordering of detection.

Comparing Eqs. (44) and (48), the two-mode correlation signal is mainly based on the channel preferentially selected by the filter, that is, it has a lot to do with the photon population of the upper and lower energy levels of the second dressed state. Due to the multiphoton correction of the weaker driving field, the population of the upper and lower energy levels of the second dressed representation is not equal. This leads to a significant asymmetry in the correlation signal when the ordering of the detection is different. Thus it is not difficult to analyze under the condition of two-photon resonance. In the case of constant driving field strength, i.e.,  $\alpha = 0.4$ , as long as the two filters are near resonance with frequency  $\omega_{if}$  and  $\omega_{jt}$  ( $j = F, R, T$ ), respectively, the correlation signals of different time ordering obtained should be exactly the same, as shown in Fig. 7(b). As the strength of the weaker driving field changes, the asymmetry of the photon's correlation signal

changes. When the value of  $\alpha$  gets bigger and bigger, namely, the strength of the weaker driving field gets stronger and stronger, the population distribution difference between the upper and lower energy levels of the second dressed state also gets bigger and bigger, as shown in Fig. 5. The asymmetry in the correlation signal of the detected photon will also increase accordingly, as shown in Figs. 7(a), 7(b), and 7(c). It is further shown that the population distribution has an important impact on the asymmetry of the correlation signal of the detected photon.

## 2. Filtering between central and sidepeaks

The method of conditional quantum states can also be used to analyze the situation of one of the filters being near resonant with the frequency of  $\omega_{i\tau}$  ( $i = F, R, T$ ), that is, one filter near-resonates with the frequency of any one of the central peaks in the nine peaks of the incoherent spectrum. Let us consider the  $a$ -mode filter centered at frequency  $\omega_{Rr}$  and the  $b$ -mode filter centered at frequency  $\omega_{Tt}$  as an example. If  $a$ -mode photons are detected at time  $t$  and  $b$ -mode photons are detected at time  $(t + \tau)$ , the time evolution operator of the conditional quantum state can be expressed as

$$\begin{aligned} \rho_{r,a}(\tau) = & \rho_{+'+'}[(|+'\rangle, 0_a, 0_b) + C_1(\tau)|-\rangle, 0_a, 1_b) \\ & * (|+'\rangle, 0_a, 0_b + C_1^*(\tau)|-\rangle, 0_a, 1_b) \\ & + |C_2(\tau)|^2|-\rangle, 0_a, 1_b\rangle\langle-\rangle, 0_a, 1_b|], \end{aligned} \quad (49)$$

with

$$\begin{aligned} C_1(\tau) = & A_{1+'}A_{1-'}[1 - e^{-\left(\frac{\kappa}{2} + i\delta_b\right)\tau}], \\ C_2(\tau) = & (-i\delta_a + i\delta_b) \frac{A_{1+'}A_{1-'}e^{-\left(\frac{\kappa}{2} + i\delta_b\right)\tau}}{\kappa + i(\delta_a + \delta_b)}, \end{aligned} \quad (50)$$

where  $A_{1+'} = -\frac{ig\Pi_0^{(0)}}{\frac{\kappa}{2} + i\delta_a}$  and  $A_{1-'} = -\frac{ig\Pi_{-2}^{(-)}}{\frac{\kappa}{2} + i\delta_b}$  are conditional probability amplitudes for reverse-time-ordering and positive-time-ordering detection for the  $b$ -mode photon, respectively.

The un-normalized two-mode and second-order correlation function is written by

$$G^{(2)}(a, b, \tau) = \rho_{+'+'}|C_1(\tau) + C_2(\tau)|^2. \quad (51)$$

Then the normalized two-mode and second-order correlation function is given by

$$\begin{aligned} g^{(2)}(a, b, \tau) = & \left| \frac{1}{\left(\frac{\kappa}{2} + i\delta_a\right)\left(\frac{\kappa}{2} + i\delta_b\right)} \left[ 1 - \frac{\left(\frac{\kappa}{2} + i\delta_a\right)e^{-\left(\frac{\kappa}{2} + i\delta_b\right)\tau}}{\kappa + i(\delta_a + \delta_b)} \right. \right. \\ & \left. \left. - \frac{\left(\frac{\kappa}{2} + i\delta_a\right)e^{-\left(\frac{\kappa}{2} + i\delta_b\right)\tau}}{\kappa + i(\delta_a + \delta_b)} \right] \right|. \end{aligned} \quad (52)$$

The same process calculates the two-mode correlation function of detecting  $b$ -mode photons, followed by detecting  $a$ -mode photons, and the normalized correlation function reads as

$$\begin{aligned} g^{(2)}(b, a, \tau) = & \left| \frac{1}{\left(\frac{\kappa}{2} + i\delta_a\right)\left(\frac{\kappa}{2} + i\delta_b\right)} \left[ 1 - \frac{\left(\frac{\kappa}{2} + i\delta_b\right)e^{-\left(\frac{\kappa}{2} + i\delta_a\right)\tau}}{\kappa + i(\delta_a + \delta_b)} \right. \right. \\ & \left. \left. - \frac{\left(\frac{\kappa}{2} + i\delta_b\right)e^{-\left(\frac{\kappa}{2} + i\delta_a\right)\tau}}{\kappa + i(\delta_a + \delta_b)} \right] \right|. \end{aligned} \quad (53)$$

First, under the condition of two-photon resonance  $\delta_a + \delta_b = 0$  and short-time detection, the two-mode second-order correlation functions obtained by Eqs. (52) and (53) are exactly the same, corresponding to the blue dotted line and red solid line in Fig. 7(d). Then we can analyze this conclusion from Fig. 8(b). The dressed atom in the two emission channels in Fig. 8(b) are triggered by common energy atomic states  $|+'\rangle$  and terminated by common energy atomic states  $|-\rangle$ , thereby establishing timing interference. Combining with Eq. (51), it is not difficult to conclude that when the filtered peak contains the central peak of any band, the correlation signal has time symmetry in short-time detection in Fig. 7(d).

In the case of  $\kappa \gg \gamma$  and  $\tau \sim \kappa^{-1} \ll \gamma^{-1}$ , the methods of wave function and conditional quantum state are used to analyze the above two complete filtering situations. The quantum filtering system preferentially selects the information of the positive time ordering, that is, the photon information with the same ordering of detection, so as to affect the two-photon correlation signals of different detection ordering. If the initial state and final state of different detection ordering channels are different, the population of the priority detection channel is the main factor, which makes the two-photon correlation signals of different timings asymmetrical; if the initial state and final state of different channels are all the same, and even if the detection ordering is different, the two-photon correlation signals still remain symmetrical.

Here we evaluate the experimental feasibility of the parameters of our system. In Ref. [29] the frequency of the central peak of the first-order harmonic for the emission spectrum of a QD dressed by a resonant laser with drive strength  $\Omega_1 = 30 \mu\text{eV}$  and a second laser with drive strength  $\Omega_2 = 20 \mu\text{eV}$  is  $\omega = 30 \mu\text{eV}$ . When analyzing incoherent spectra in Sec. IID, our theoretical parameter is  $2\Omega_1 = 50\gamma$ , and when  $\alpha = 0.6$ , the theoretically calculated spectra are basically consistent with the experimental result. In Ref. [57], it mentions that in order to ensure that the correlation peaks of the three photons can be observed separately,  $\Omega/2\pi = 15 \text{ GHz}$  for the radiative linewidth of a single quantum dot  $\Omega/2\pi = 0.2 \text{ GHz}$ , i.e.,  $\Omega = 75\gamma$ . When discussing the two-photon statistical signal of the system in Sec. III, the parameters of our system are  $2\Omega = 80\gamma$ ,  $\kappa = 0.8\gamma$ . At present, the photon statistical properties of two photons, three photons, and even  $n$ -photons of a two-level atom driven by a single laser have been fully studied, both experimentally and theoretically [2,57,58]. It is worth noting that, so far, most of the theoretical and experimental photon statistical properties show obvious symmetry [37–39]. Therefore our theoretical model provides a feasible theoretical support for the experimental observation of asymmetric two-photon correlation of the two-level atomic system driven by the bichromatic field.

## IV. CONCLUSIONS

We fully study the fluorescence spectrum and frequency-resolved photon statistics of bichromatically driven two-level atoms. Through the Schrieffer-Wolff perturbation theory and the effective Hamiltonian theory, the multiphoton effect of the weaker driving field is intuitively revealed, which affects the energy and coherence of the system and the physical nature of spontaneous emission. The physical origin of

unequal energy-level population distribution and the physical picture of spectral asymmetry are further revealed. The Raman two-photon process and the cascaded two-photon process of the weaker driving field have opposite effects on the opposite sidepeaks of the central band, the central peak of the first-order harmonic, and the opposite sidepeaks of the second-order harmonic, so that the fluorescence spectrum appears to have obvious asymmetry. The second-order and third-order corrections of the weaker driving field have a greater influence on the higher-order harmonics. Therefore, as the strength of the weaker driving field increases, so does the strength of the higher-order harmonics of the fluorescence spectrum. Our analytical results are basically consistent with the numerical solutions of Ficek and Freedhoff [18] and the experimental results of Gustin *et al.* [29]. Next, the influence of the multiphoton effect of the weaker driving field on the frequency-resolved photon correlation signals between different components of the spectra is discussed in detail. To fully reveal the physical source of the asymmetry of the time-domain correlation signal, two methods of correlation moment and conditional quantum state are used to analyze the frequency-resolved timing detection process.

These results of ours further suggest that the impact of multiphoton effects on fluorescence spectra and photon statistics is important and not negligible in strongly coupled systems. Our work is not limited to natural atomic systems but has a certain theoretical guiding significance for the study of quantum manipulation [59] and quantum simulation [60] based on multichromatically driven technology in solid-state devices such as quantum dots.

#### ACKNOWLEDGMENTS

This work is supported by the National Natural Science Foundation of China (Grant No. 12174139).

#### APPENDIX: THE EXPANSION OF THE TRANSITION OPERATOR IN THE DRESSED REPRESENTATION

In Sec. II C the atomic operator of the third-order perturbation in the first dressed representation is

$$\sigma_- \rightarrow \sum_{\substack{j=0,\pm \\ k=0,\dots,\pm 4}} [M_{2k}^{(j)} R_j] e^{2ik\Omega t}, \quad (\text{A1})$$

where the specific expanded form of the transition weight is given by Eq. (A2). The effects of the opposite first-order correction on the opposite sidepeaks of the central band by the cascaded two-photon process and the Raman two-photon process of the weaker driving field are analyzed in detail. Figure 9 analyzes the first-order correction of the weak driving field to the high-frequency transition of spontaneous emission.

Figure 9(a) is the first-order correction of  $M_2^{(0)}$  and  $M_{-2}^{(0)}$  by the weaker driving field. Take channel (1) as an example. The dressed atom absorbs a photon of frequency  $\omega_2$  from the weaker driving field and transits from the initial state  $|+\rangle$  to the intermediate state  $|-\rangle$ . Since the single photon nonresonates, it immediately emits a photon of frequency

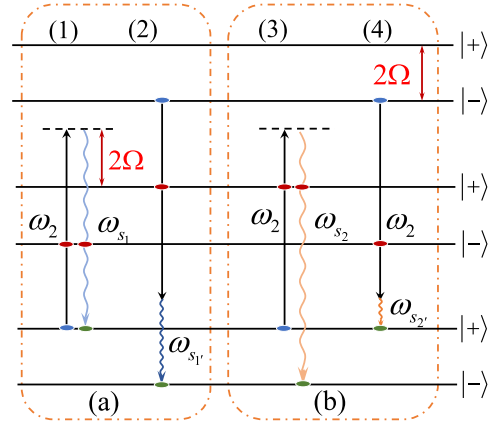


FIG. 9. First-order correction process for  $n$ -order harmonics by weaker driving field ( $n=1,2$ ). The solid arrow represents the emitted or absorbed photon of frequency  $\omega_2$ . The wavy arrow represents the frequency of the radiated fluorescence,  $\omega_{s1}$ ,  $\omega_{s1'}$ : two first-order harmonic sidepeak frequencies;  $\omega_{s2}$ ,  $\omega_{s2'}$ : two second-order harmonic sidepeak frequencies. Blue ellipse: initial state; red ellipse: intermediate state; green ellipse: final states. (a) First-order correction of the weaker driving field for first-order harmonic; (b) first-order correction of the weaker driving field for second-order harmonic.

$\omega_1 + 2\Omega$  back to the initial state  $|+\rangle$ , completing a Raman two-photon transition. The weight of the dressed atom to complete the transition  $R_{++} = |+\rangle\langle +|$  corresponds to the first term in  $M_{-2}^{(0)}$ , which is the first-order correction of the weaker driving field. The cascaded two-photon transition of channel (2) corresponds to the first term in  $M_2^{(0)}$ , which is a first-order correction of the weaker driving field. The dressed atom emits a photon of frequency  $\omega_2$  from the initial state  $|-\rangle$  and then immediately emits a photon of frequency  $\omega_1 - 2\Omega$  to the final state  $|-\rangle$  to the weaker driving field, due to single photon nonresonance. Complete a cascaded two-photon transition  $R_{--} = |-\rangle\langle -|$ . It can be seen that the first-order corrections of  $M_2^{(0)}$  and  $M_{-2}^{(0)}$  by the cascaded and Raman two-photon processes are opposite, which is also the main reason for the asymmetry of the central peak of the first-order harmonic of the spectrum. In the same analysis, the Raman two-photon process of channel (3) and the cascaded two-photon process of channel (4) in Fig. 9(b) correspond to the first-order correction of  $M_{-4}^{(-)}$  and  $M_4^{(+)}$  by the weaker driving field.

Take channel (3) as an example. The dressed atom absorbs a photon of frequency  $\omega_2$ , then immediately emits a fluorescent photon of frequency  $\omega_1 + 4\Omega$ . This Raman two-photon process corresponds to a first-order correction of  $M_{-4}^{(-)}$  by the weaker driving field. The two-photon process of the weaker driving field in channel (3) and channel (4) has the opposite effect on  $M_{-4}^{(-)}$  and  $M_4^{(+)}$ , which makes the opposite sidepeaks of the second-order harmonic of the spectrum show asymmetry. It can be seen from Eqs. (A2) and (A3) that the second-order and third-order corrections of the weaker driving field have a greater influence on the higher-order harmonics in the spectrum. As shown in Fig. 6, as the strength of the weaker driving field increases, the strength of the higher-order harmonics will also increase accordingly.

The specific expansion of the transition weights of the dressed atom in the first dressed representation and the second dressed representation are as follows:

$$M_0^{(0)} = \frac{1}{2} - \frac{\alpha^2}{64}, \quad M_0^{(+)} = \frac{\alpha}{4} + \frac{77\alpha^3}{1536}, \quad (\text{A2a})$$

$$M_0^{(-)} = -\frac{\alpha}{4} + \frac{17\alpha^3}{1536}, \quad M_2^{(0)} = -\frac{\alpha}{16} - \frac{55\alpha^3}{3072}, \quad (\text{A2b})$$

$$M_2^{(+)} = -\frac{1}{2} - \frac{15\alpha^2}{128}, \quad M_2^{(-)} = -\frac{3\alpha^2}{64}, \quad (\text{A2c})$$

$$M_{-2}^{(0)} = \frac{\alpha}{16} + \frac{215\alpha^3}{3072}, \quad M_{-2}^{(-)} = \frac{1}{2} - \frac{49\alpha^2}{128} \quad (\text{A2d})$$

$$M_{-2}^{(+)} = -\frac{13\alpha^2}{64}, \quad M_4^{(0)} = -\frac{5\alpha^2}{96}, \quad (\text{A2e})$$

$$M_4^{(+)} = -\frac{\alpha}{8} - \frac{25\alpha^3}{384}, \quad M_4^{(-)} = \frac{35\alpha^3}{2304}, \quad (\text{A2f})$$

$$M_{-4}^{(0)} = \frac{5\alpha^2}{96}, \quad M_{-4}^{(+)} = \frac{55\alpha^3}{2304}, \quad (\text{A2g})$$

$$M_{-4}^{(-)} = \frac{3\alpha}{8} - \frac{11\alpha^3}{384}, \quad M_6^{(0)} = -\frac{47\alpha^3}{6144}, \quad (\text{A2h})$$

$$M_6^{(+)} = -\frac{5\alpha^2}{384}, \quad M_{-6}^{(0)} = \frac{239\alpha^3}{6144}, \quad (\text{A2i})$$

$$M_{-6}^{(-)} = \frac{37\alpha^2}{384}, \quad M_8^{(+)} = -\frac{7\alpha^3}{9216}, \quad (\text{A2j})$$

$$M_{-8}^{(-)} = \frac{97\alpha^3}{9216}. \quad (\text{A2k})$$

The transition weight of the dressed atom in the second dressed representation is as follows:

$$\Pi_0^{(0)} = \left(\frac{1}{2} - \frac{\alpha^2}{64}\right)(c_2^2 - s_2^2) - \frac{47\alpha^3}{768}s_2c_2, \quad (\text{A3a})$$

$$\Pi_0^{(-)} = \left(1 - \frac{\alpha^2}{32}\right)s_2c_2 - \frac{\alpha}{4} + \frac{17\alpha^3}{1536}c_2^2 - \frac{77\alpha^3}{1536}s_2^2, \quad (\text{A3b})$$

$$\Pi_0^{(+)} = \left(1 - \frac{\alpha^2}{32}\right)s_2c_2 + \frac{\alpha}{4} - \frac{17\alpha^3}{1536}s_2^2 + \frac{77\alpha^3}{1536}c_2^2, \quad (\text{A3c})$$

$$\Pi_2^{(0)} = \left(-\frac{1}{2} + \frac{75\alpha^2}{128}\right)s_2c_2 + \left(\frac{\alpha}{16} + \frac{215\alpha^3}{3072}\right)(c_2^2 - s_2^2), \quad (\text{A3d})$$

$$\Pi_2^{(-)} = \left(\frac{1}{2} - \frac{49\alpha^2}{128}\right)c_2^2 + \left(\frac{\alpha}{8} + \frac{215\alpha^3}{1536}\right)s_2c_2 + \frac{13\alpha^3}{64}s_2^2, \quad (\text{A3e})$$

$$\Pi_2^{(+)} = \left(-\frac{1}{2} + \frac{49\alpha^2}{128}\right)s_2^2 + \left(\frac{\alpha}{8} + \frac{215\alpha^3}{1536}\right)s_2c_2 - \frac{13\alpha^3}{64}c_2^2, \quad (\text{A3f})$$

$$\Pi_{-2}^{(0)} = -\left(\frac{\alpha}{16} + \frac{55\alpha^3}{3072}\right)(c_2^2 - s_2^2) + \left(\frac{1}{2} + \frac{21\alpha^2}{128}\right)s_2c_2, \quad (\text{A3g})$$

$$\Pi_{-2}^{(-)} = -\left(\frac{\alpha}{8} + \frac{55\alpha^3}{1536}\right)s_2c_2 + \frac{3\alpha^3}{64}s_2^2 - \left(\frac{1}{2} + \frac{15\alpha^2}{128}\right)c_2^2, \quad (\text{A3h})$$

$$\Pi_{-2}^{(+)} = -\left(\frac{\alpha}{8} + \frac{55\alpha^3}{1536}\right)s_2c_2 - \frac{3\alpha^3}{64}c_2^2 + \left(\frac{1}{2} + \frac{15\alpha^2}{128}\right)s_2^2, \quad (\text{A3i})$$

$$\Pi_4^{(0)} = \frac{5\alpha^2}{96}(c_2^2 - s_2^2) + \left(-\frac{3\alpha}{8} + \frac{11\alpha^3}{2304}\right)s_2c_2, \quad (\text{A3j})$$

$$\Pi_4^{(-)} = \frac{5\alpha^2}{48}s_2c_2 - \frac{55\alpha^3}{2304}s_2^2 - \left(-\frac{3\alpha}{8} + \frac{11\alpha^3}{384}\right)c_2^2, \quad (\text{A3k})$$

$$\Pi_4^{(+)} = \frac{5\alpha^2}{48}s_2c_2 + \frac{55\alpha^3}{2304}c_2^2 + \left(-\frac{3\alpha}{8} + \frac{11\alpha^3}{384}\right)s_2^2, \quad (\text{A3l})$$

$$\Pi_{-4}^{(0)} = -\frac{5\alpha^2}{96}(c_2^2 - s_2^2) + \left(\frac{\alpha}{8} + \frac{115\alpha^3}{2304}\right)s_2c_2, \quad (\text{A3m})$$

$$\Pi_{-4}^{(-)} = -\frac{5\alpha^2}{48}s_2c_2 + \frac{35\alpha^3}{2304}c_2^2 + \left(\frac{\alpha}{8} + \frac{25\alpha^3}{384}\right)s_2^2, \quad (\text{A3n})$$

$$\Pi_{-4}^{(+)} = -\frac{5\alpha^2}{48}s_2c_2 - \frac{35\alpha^3}{2304}s_2^2 - \left(\frac{\alpha}{8} + \frac{25\alpha^3}{384}\right)c_2^2, \quad (\text{A3o})$$

$$\Pi_6^{(0)} = -\frac{37\alpha^2}{384}s_2c_2 + \frac{239\alpha^3}{6144}(c_2^2 - s_2^2), \quad (\text{A3p})$$

$$\Pi_6^{(-)} = \frac{37\alpha^2}{384}c_2^2 + \frac{239\alpha^3}{3072}s_2c_2, \quad (\text{A3q})$$

$$\Pi_6^{(+)} = -\frac{37\alpha^2}{384}s_2^2 + \frac{239\alpha^3}{3072}s_2c_2, \quad (\text{A3r})$$

$$\Pi_{-6}^{(0)} = \frac{5\alpha^2}{384}s_2c_2 - \frac{47\alpha^3}{6144}(c_2^2 - s_2^2), \quad (\text{A3s})$$

$$\Pi_{-6}^{(-)} = \frac{5\alpha^2}{384}s_2 - \frac{47\alpha^3}{3072}s_2c_2, \quad (\text{A3t})$$

$$\Pi_{-6}^{(+)} = -\frac{5\alpha^2}{384}c_2 - \frac{47\alpha^3}{3072}s_2c_2, \quad (\text{A3u})$$

$$\Pi_8^{(0)} = -\frac{97\alpha^3}{9216}s_2c_2, \quad \Pi_8^{(-)} = \frac{97\alpha^3}{9216}c_2^2, \quad (\text{A3v})$$

$$\Pi_8^{(+)} = -\frac{97\alpha^3}{9216}s_2^2, \quad \Pi_{-8}^{(0)} = \frac{7\alpha^3}{9216}s_2c_2, \quad (\text{A3w})$$

$$\Pi_{-8}^{(-)} = \frac{7\alpha^3}{9216}s_2^2, \quad \Pi_{-8}^{(+)} = -\frac{7\alpha^3}{9216}c_2^2. \quad (\text{A3x})$$

[1] N. Somaschi, V. Giesz, L. De Santis, J. C. Loredano, M. P. Almeida, G. Hornecker, S. L. Portalupi, T. Grange, C. Antón, J. Demory, C. Gómez, I. Sagnes, N. D. Lanzillotti-Kimura, A. Lemaitre, A. Auffeves, A. G. White, L. Lanco, and P. Senellart, *Nat. Photon.* **10**, 340 (2016).

[2] A. Ulhaq, S. Weiler, S. M. Ulrich, R. Roßbach, M. Jetter, and P. Michler, *Nat. Photon.* **6**, 238 (2012).

[3] T. Hönigl-Decrinis, R. Shaikhaidarov, S. E. de Graaf, V. N. Antonov, and O. V. Astafiev, *Phys. Rev. Appl.* **13**, 024066 (2020).

- [4] T. D. Ladd, F. Jelezko, R. Laflamme, Y. Nakamura, C. Monroe, and J. L. O'Brien, *Nature (London)* **464**, 45 (2010).
- [5] S. Ates, S. M. Ulrich, S. Reitzenstein, A. Löffler, A. Forchel, and P. Michler, *Phys. Rev. Lett.* **103**, 167402 (2009).
- [6] S. M. Ulrich, S. Ates, S. Reitzenstein, A. Löffler, A. Forchel, and P. Michler, *Phys. Rev. Lett.* **106**, 247402 (2011).
- [7] C. Roy and S. Hughes, *Phys. Rev. Lett.* **106**, 247403 (2011).
- [8] C. Roy and S. Hughes, *Phys. Rev. B* **85**, 115309 (2012).
- [9] M. Peiris, K. Konthasinghe, Y. Yu, Z. C. Niu, and A. Muller, *Phys. Rev. B* **89**, 155305 (2014).
- [10] Y. He, Y.-M. He, J. Liu, Y.-J. Wei, H. Y. Ramírez, M. Atatüre, C. Schneider, M. Kamp, S. Höfling, C.-Y. Lu, and J.-W. Pan, *Phys. Rev. Lett.* **114**, 097402 (2015).
- [11] P. Senellart, G. Solomon, and A. White, *Nat. Nanotechnol.* **12**, 1026 (2017).
- [12] D. M. Toyli, A. W. Eddins, S. Boutin, S. Puri, D. Hover, V. Bolkhovskiy, W. D. Oliver, A. Blais, and I. Siddiqi, *Phys. Rev. X* **6**, 031004 (2016).
- [13] S. Rohr, E. Dupont-Ferrier, B. Pigeau, P. Verlot, V. Jacques, and O. Arcizet, *Phys. Rev. Lett.* **112**, 010502 (2014).
- [14] A. Mohammadzadeh and M. F. Miri, *Phys. Rev. B* **99**, 115440 (2019).
- [15] J. Pan, H. Z. Jooya, G. Sun, Y. Fan, P. Wu, D. A. Telnov, S.-I. Chu, and S. Han, *Phys. Rev. B* **96**, 174518 (2017).
- [16] D. L. Aronstein, R. S. Bennink, R. W. Boyd, and C. R. Stroud, *Phys. Rev. A* **65**, 067401 (2002).
- [17] C. C. Yu, J. R. Bochinski, T. M. V. Kordich, T. W. Mossberg, and Z. Ficek, *Phys. Rev. A* **56**, R4381 (1997).
- [18] Z. Ficek and H. S. Freedhoff, *Phys. Rev. A* **53**, 4275 (1996).
- [19] Y. Ota, S. Iwamoto, N. Kumagai, and Y. Arakawa, *Phys. Rev. Lett.* **107**, 233602 (2011).
- [20] T. Rudolph, H. S. Freedhoff, and Z. Ficek, *J. Opt. Soc. Am. B* **15**, 2325 (1998).
- [21] Y. Zhu, Q. Wu, A. Lezama, D. J. Gauthier, and T. W. Mossberg, *Phys. Rev. A* **41**, 6574 (1990).
- [22] G. Y. Kryuchkov, *Opt. Commun.* **54**, 19 (1985).
- [23] W. M. Ruyten, *Phys. Rev. A* **40**, 1447 (1989).
- [24] H. Freedhoff and Z. Chen, *Phys. Rev. A* **41**, 6013 (1990).
- [25] S. P. Tewari and M. K. Kumari, *Phys. Rev. A* **41**, 5273 (1990).
- [26] G. S. Agarwal, Y. Zhu, D. J. Gauthier, and T. W. Mossberg, *J. Opt. Soc. Am. B* **8**, 1163 (1991).
- [27] Z. Ficek and H. S. Freedhoff, *Phys. Rev. A* **48**, 3092 (1993).
- [28] A. Papageorge, A. Majumdar, E. D. Kim, and J. Vučković, *New J. Phys.* **14**, 013028 (2012).
- [29] C. Gustin, L. Hanschke, K. Boos, J. R. A. Müller, M. Kremser, J. J. Finley, S. Hughes, and K. Müller, *Phys. Rev. Res.* **3**, 013044 (2021).
- [30] J. R. Schrieffer and P. A. Wolff, *Phys. Rev.* **149**, 491 (1966).
- [31] C. E. Soliveres, *Phys. Rev. A* **24**, 4 (1981).
- [32] H.-S. Chou and J. Evers, *Phys. Rev. Lett.* **104**, 213602 (2010).
- [33] I. K. Kominis, G. Koliopoulos, D. Charalambidis, and P. Tzallas, *Phys. Rev. A* **89**, 063827 (2014).
- [34] Á. Gombkötő, S. Varró, P. Mati, and P. Földi, *Phys. Rev. A* **101**, 013418 (2020).
- [35] Á. Gombkötő, P. Földi, and S. Varró, *Phys. Rev. A* **104**, 033703 (2021).
- [36] C. Brif, R. Chakrabarti, and H. Rabitz, *New J. Phys.* **12**, 075008 (2010).
- [37] C. L. Phillips, A. J. Brash, D. P. S. McCutcheon, J. Iles-Smith, E. Clarke, B. Royall, M. S. Skolnick, A. M. Fox, and A. Nazir, *Phys. Rev. Lett.* **125**, 043603 (2020).
- [38] L. Hanschke, L. Schweickert, J. C. L. Carreño, E. Schöll, K. D. Zeuner, T. Lettner, E. Z. Casalengua, M. Reindl, S. F. C. da Silva, R. Trotta, J. J. Finley, A. Rastelli, E. del Valle, F. P. Laussy, V. Zwiller, K. Müller, and K. D. Jöns, *Phys. Rev. Lett.* **125**, 170402 (2020).
- [39] M. Jakob and G. Y. Kryuchkyan, *Phys. Rev. A* **61**, 053823 (2000).
- [40] C. Sánchez Muñoz and F. Schlawin, *Phys. Rev. Lett.* **124**, 203601 (2020).
- [41] Y. Ben-Aryeh, H. Freedhoff, and T. Rudolph, *J. Opt. B: Quantum semiclass. Opt.* **1**, 624 (1999).
- [42] E. del Valle, A. Gonzalez-Tudela, F. P. Laussy, C. Tejedor, and M. J. Hartmann, *Phys. Rev. Lett.* **109**, 183601 (2012).
- [43] D. Cano, *J. Phys. B: At. Mol. Opt. Phys.* **54**, 045502 (2021).
- [44] M. Malekakhlagh, E. Magesan, and D. C. McKay, *Phys. Rev. A* **102**, 042605 (2020).
- [45] M. Malekakhlagh, E. Magesan, and L. C. G. Govia, *Phys. Rev. A* **106**, 052601 (2022).
- [46] J. A. Blackmore, R. Sawant, P. D. Gregory, S. L. Bromley, J. Aldegunde, J. M. Hutson, and S. L. Cornish, *Phys. Rev. A* **102**, 053316 (2020).
- [47] D. Chetty, R. D. Glover, B. A. deHarak, X. M. Tong, H. Xu, T. Pauly, N. Smith, K. R. Hamilton, K. Bartschat, J. P. Ziegel, N. Douguet, A. N. Luiten, P. S. Light, I. V. Litvinyuk, and R. T. Sang, *Phys. Rev. A* **101**, 053402 (2020).
- [48] K. Totsuka and M. Tomita, *Phys. Rev. B* **59**, 11139 (1999).
- [49] G.-X. Li, H.-T. Tan, and M. Macovei, *Phys. Rev. A* **76**, 053827 (2007).
- [50] G.-x. Li, F.-l. Li, and S.-y. Zhu, *Phys. Rev. A* **64**, 013819 (2001).
- [51] M. O. Scully and M. S. Zubairy, *Quantum Optics* (Cambridge University Press, Cambridge, England, 1997).
- [52] G. Wang, Y.-X. Liu, and P. Cappellaro, *Phys. Rev. A* **103**, 022415 (2021).
- [53] G. Nienhuis, *Phys. Rev. A* **47**, 510 (1993).
- [54] Z.-a. Peng, G.-q. Yang, Q.-l. Wu, and G.-x. Li, *Phys. Rev. A* **98**, 043828 (2018).
- [55] Z.-a. Peng, G.-q. Yang, Q.-l. Wu, and G.-x. Li, *Phys. Rev. A* **99**, 033819 (2019).
- [56] C. A. Schrama, G. Nienhuis, H. A. Dijkerman, C. Steijsiger, and H. G. M. Heideman, *Phys. Rev. A* **45**, 8045 (1992).
- [57] Y. Nieves and A. Muller, *Phys. Rev. B* **98**, 165432 (2018).
- [58] Y. Nieves and A. Muller, *Phys. Rev. B* **102**, 155418 (2020).
- [59] G. Balasubramanian, P. Neumann, D. Twitchen, M. Markham, R. Kolesov, N. Mizuochi, J. Isoya, J. Achard, J. Beck, J. Tissler, V. Jacques, P. R. Hemmer, F. Jelezko, and J. Wrachtrup, *Nat. Mater.* **8**, 383 (2009).
- [60] J. L. O'Brien, A. Furusawa, and J. Vučković, *Nat. Photon.* **3**, 687 (2009).